COMMUNICATION

Check for updates

Electronic properties of phases in the quasi-binary Bi₂Se₃–Bi₂S₃ system

Zipporah Rini Benher, [ID] [a] Sandra Gardonio, [ID] *[a] Mattia Fanetti, [ID] [a]
Paolo Moras, [ID] [b] Asish K. Kundu, [ID] [b] Chiara Bigi[c] and Matjaz Valant [ID] [ad]

We explored the properties of the quasi-binary Bi_2Se_3–Bi_2S_3 system over a wide compositional range. X-ray diffraction analysis demonstrates that rhombohedral crystals can be synthesized within the solid solution interval 0–22 mol% Bi_2S_3, while at 33 mol% Bi_2S_3 only orthorhombic crystals are obtained. Core level photoemission spectroscopy reveals the presence of Bi^{3+}, Se^{2-} and S^{2-} species and the absence of metallic species, thus indicating that S incorporation into Bi_2Se_3 proceeds prevalently through the substitution of Se with S. Spin- and angle-resolved photoemission spectroscopy shows that topological surface states develop on the surfaces of the $Bi_2Se_{3-y}S_y$ ($y \leq 0.66$) rhombohedral crystals, in close analogy with the prototypical case of Bi_2Se_3, while the orthorhombic crystals with higher S content turn out to be trivial semiconductors. Our results connect unambiguously the phase diagram and electronic properties of the Bi_2Se_3–Bi_2S_3 system.

Introduction

Topological insulators (TIs) are a new class of materials possessing a bulk band gap, like ordinary band insulators, and protected conducting states on their edges, such as their surfaces. These states, known as Topological Surface States (TSSs), appear because of a combination of spin–orbit coupling and time reversal symmetry.[1] TSSs of TIs display a linear energy–momentum $E(k_{\parallel})$ relation, which is characteristic of Dirac electrons, and spin-momentum locking, resulting in spin-polarized transport on the surface/edge and significant suppression of backscattering by impurities and defects. These properties make TIs attractive for a variety of nano electronic applications such as spin-transfer torque non-volatile memories[2] and field-effect transistors,[3] but also in the

field of optoelectronics for helicity-dependent photocurrents[4,5] and catalysis.[6]

Bi_2Se_3 and Bi_2Te_3 belong to a class of compounds called tetradymites and are considered as the three-dimensional prototypical TI materials. Ternary variants such as Bi_2Te_2Se, Bi_2Se_2Te and Bi_2Te_2S have also been investigated due to their superior bulk insulating properties with respect to their binary counterparts.[7–10] In this context calculations have predicted Bi_2Se_2S to be a stable TI in its stoichiometric form,[11,12] but the few available experimental results are not yet conclusive with respect to this issue. From the material's point of view, it is known that Bi_2S_3 has an orthorhombic crystalline structure with trivial insulating properties, while Bi_2Se_3 has a rhombohedral crystalline structure. The Bi_2Se_3–Bi_2S_3 phase diagram shows that these two compounds form two solid solutions over a large composition range. At room temperature the orthorhombic solid solution extends from 0 to ∼67 mol% Bi_2Se_3 and the rhombohedral from 0 to 16 mol% Bi_2S_3. A two-phase range exists between the solid solutions. An eutectic composition was found at 23 mol% Bi_2S_3 with the eutectic temperature at around 680 °C[13,14] (Fig. 1(b)).

Recently, transport measurements on $Bi_2Se_{3-y}S_y$ with $0 \leq y \leq 0.21$ indicated the existence of a TSS accompanied by unusual negative magnetoresistance behaviour.[15] In a study of the $Sr_xBi_2Se_{3-y}S_y$ alloy ($x = 0.066$ and $0 \leq y \leq 0.4$), it has been indirectly proved that sulphur destroys TSSs and suppresses superconductivity of $Sr_xBi_2Se_3$ as a result of a sulphur occupational disorder.[16]

Angle-resolved photoemission spectroscopy (ARPES) has been used to probe in a direct way the electronic structures of different ternary chalcogenides.[17] The available ARPES results show that Bi_2Se_2S is not a topological insulator[17] in contrast with the theoretical prediction.[11,12] This result is interpreted as a consequence of the fact that the solid solution $Bi_2Se_{3-y}S_y$ prefers the rhombohedral structure at higher concentration of heavier Se, and the orthorhombic structure at higher concentration of lighter S.

Overall, a picture that reconciles the theoretical and experimental results on the topological properties of the Bi_2Se_3–Bi_2S_3

[a] Materials Research Laboratory, Univerza v Novi Gorici, Vipaska 11c, Ajdovščina 5270, Slovenia. E-mail: sandra.gardonio@ung.si

[b] Istituto di Struttura della Materia-CNR (ISM-CNR), S.S. 14, km 163.5, Trieste I-34149, Italy

[c] CNR-IOM Laboratorio TASC, Trieste I-34149, Italy

[d] Institute of Fundamental and Frontier Sciences, University of Electronic Science and Technology of China, Chengdu 610054, China

3058 | *J. Mater. Chem. C*, 2021, **9**, 3058–3064

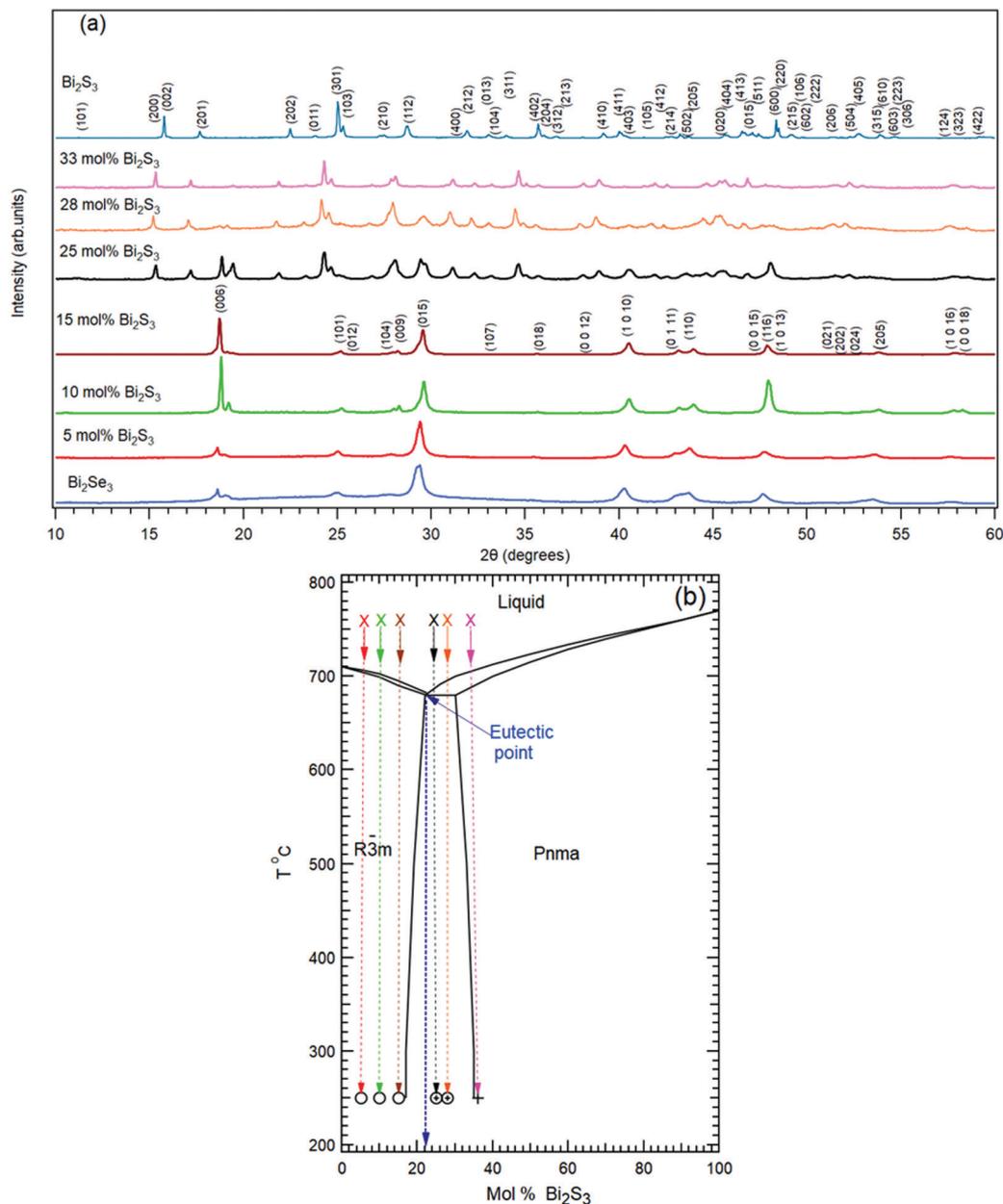This journal is © The Royal Society of Chemistry 2021

Fig. 1 (a) Powder XRD patterns measured on the samples extracted from the ingots with different nominal mol% of Bi_2S_3 as indicated in (b). The measured patterns of pure Bi_2Se_3 and Bi_2S_3 corresponding to PDF #00-033-0214 and PDF #03-065-2431 respectively are reported. (b) Phase diagram of $Bi_2S_3-Bi_2Se_3$.[14] Crosses represent the liquid phase, open circles the rhombohedral phase and plus signs the orthorhombic phase.

quasi-binary compounds is still lacking. We revisited the electronic properties of these systems along the entire compositional tie line with the use of bulk sensitive technique X-ray diffraction (XRD) and surface sensitive techniques low energy electron diffraction (LEED), scanning electron microscopy (SEM) with energy dispersive X-ray spectroscopy (EDX), X-ray photoemission spectroscopy (XPS) and ARPES. Spin-resolved ARPES was also employed to access the spin structure of the compounds. We show that rhombohedral single crystal structures are obtained only within the solid solution interval 0 – 22% mol of Bi_2S_3. All these systems possess spin polarized TSSs, in close analogy with the parent Bi_2Se_3 TI.

Experimental details

Bismuth and selenium were purchased from Sigma Aldrich. Sulphur was purchased from Acros Organics. Bi and S were 99.999% trace metal basis while Se was ≥99.5% trace metal basis. High quality single crystals along the $Bi_2Se_3-Bi_2S_3$ compositional tie line were grown by the Bridgman method. Stoichiometric amounts of high purity elements were sealed in evacuated quartz ampoules and heated up to 750 °C at 21 °C h^{-1}. The ampoules were maintained at that temperature for 48 h. Thereupon the temperature was slowly reduced to 250 °C at 5 °C h^{-1} and then cooled down to room temperature.
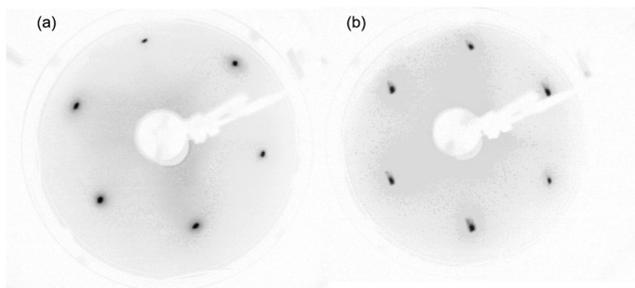
Fig. 2 LEED pattern measured on (a) Bi_2Se_3 and (b) $Bi_2Se_{2.34}S_{0.66}$ at primary electron energy of 66 eV.

Table 1 Composition of the samples analyzed in the present study

Nominal composition of the charge (Bi_2S_3 mol%)	Measured composition from EDX spectra (Bi_2S_3 mol%)	Calculated y from EDX spectra
5	3.8 ± 0.4	0.11 ± 0.01
10	10.8 ± 0.9	0.32 ± 0.03
15	14.3 ± 0.4	0.43 ± 0.01
25	22 ± 1	0.66 ± 0.03
33	36.7 ± 1.3	1.10 ± 0.04

Seven different charges were prepared: pure Bi_2Se_3, 5 mol% Bi_2S_3, 10 mol% Bi_2S_3, 15 mol% Bi_2S_3, 25 mol% Bi_2S_3, 28 mol% Bi_2S_3, 33 mol% Bi_2S_3 and pure Bi_2S_3.

The XRD patterns of the powdered samples were collected with Rigaku Miniflex600 apparatus. The chemical composition was determined by fitting the EDX spectra measured with Oxford XMax-80 apparatus (with Aztech acquisition and analysis software) installed on a Jeol JSM-7100F field-emission SEM. Table 1 reports the nominal composition of the charges,

composition estimated from the EDX analysis and corresponding y value in the chemical formula $Bi_2Se_{3-y}S_y$ of the samples studied by means of photoemission spectroscopy (see Fig. 3–6).

The photoemission experiments were carried out at Elettra synchrotron, Trieste, Italy on clean surfaces obtained by cleaving the samples *in situ* in ultra-high vacuum with pressure lower than 1.2×10^{-10} mbar. LEED was used to monitor the crystalline structure and quality of the surface. The XPS experiments were carried out at a VUV-Photoemission beamline using a Scienta R4000 hemispherical electron energy analyzer. All the XPS spectra were measured at room temperature using photon energy of 650 eV with a total energy resolution of ~ 200 meV. S 2p and Se 3s core level spectra were fitted using Voigt functions. The ARPES measurements were carried out at the APE-LE beamline using a VG Scienta DA30 hemispherical electron energy analyzer. The spin-resolved ARPES measurements were performed with the Very Low Energy Electron Diffraction B (VLEED-B) polarimeter in the in-plane magnetization configuration (spin parallel to the sample surface in the direction perpendicular to the analyzer slit, *i.e.* perpendicular to the angular dispersion direction).[18] The measurements were carried out in a 30° angular mode. The electron energy analyzer is mounted 45° with respect to the photon beam direction and the spectra collected near normal emission. ARPES and spin-resolved ARPES measurements were carried out with an overall energy resolution of 40 meV and 100 meV energy resolution respectively.

Results and discussion

The crystalline structure of the samples was analyzed by powder XRD (Fig. 1(a)).
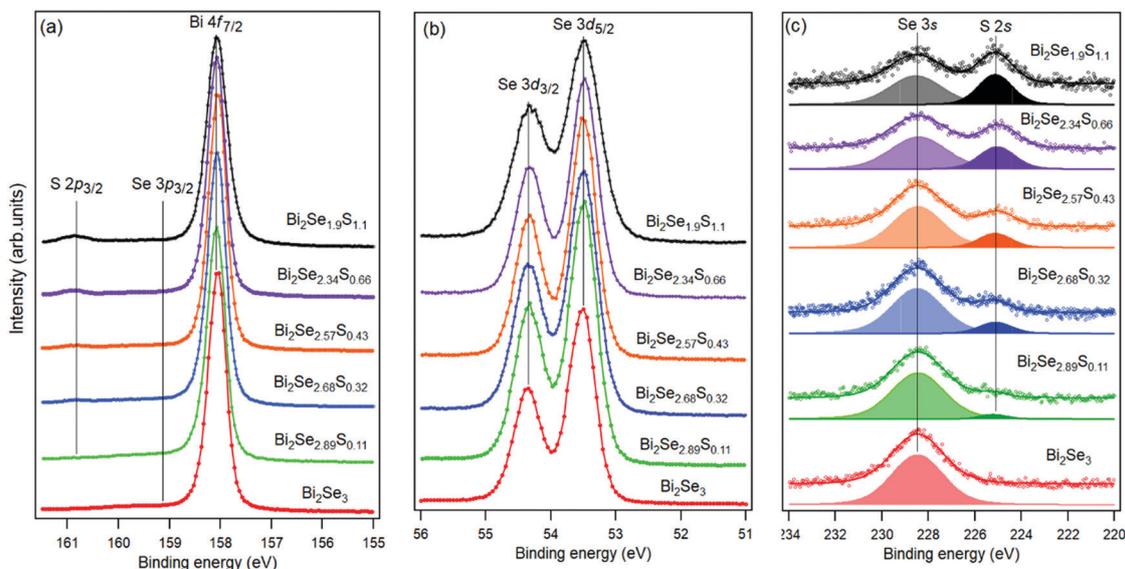

Fig. 3 Bi 4f, Se 3d, Se 3s and S 2s core level spectra measured on the samples extracted from the charges with the composition indicated in the figures. Fitting curves are reported in the case of Se 3s and S 2s core levels. In the energy region of Bi 4f, the peaks corresponding to S 2p and Se 3p core levels are also visible with very low intensity.
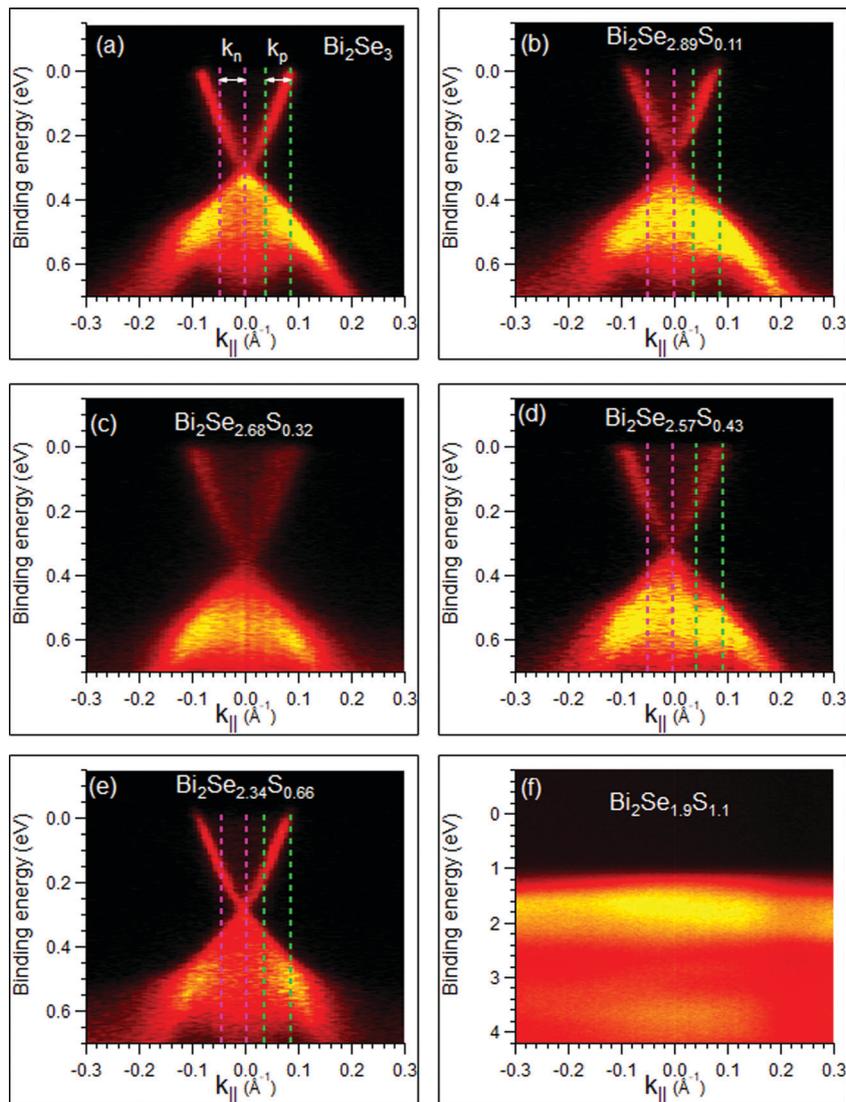
3060 | *J. Mater. Chem. C*, 2021, **9**, 3058–3064

This journal is © The Royal Society of Chemistry 2021

Fig. 4 Electronic band structure measured near E_F by means of ARPES on different $Bi_2Se_{3-y}S_y$ samples. Maps (a–e) were measured with $h\nu$ = 50 eV, and map (f) with $h\nu$ = 45 eV. $k_{\parallel}$ = 0 Å^{-1} represents the Γ point. Dashed lines in panel (a,b,d and e) delimit stripes of the photoemission map of width $\Delta k_{\parallel}$ = 0.048 Å^{-1} and centered at k_n = −0.03 Å^{-1} and k_p = +0.06 Å^{-1}. EDC$_{m\uparrow\downarrow}$ were collected within these stripes (in order to increase the signal to noise ratio) and used to extract the SEDCs reported in Fig. 6(a)–(h) (see text).

The samples corresponding to the pure Bi_2Se_3 composition and the nominal compositions with 5, 10 and 15 mol% of Bi_2S_3 were found to crystallize in the rhombohedral structure (Fig. 1(a)). EDX analysis of the single crystals extracted from the ingots showed that they possess a homogeneous chemical composition corresponding to the nominal composition of the charges. The XRD patterns of the samples with 25 and 28 mol% of Bi_2S_3 showed diffraction peaks corresponding to both the orthorhombic and rhombohedral structure. The coexistence of the two different phases is in accordance with the Bi_2S_3–Bi_2Se_3 phase diagram (Fig. 1(b))[14] where the two-phase (orthorhombic and rhombohedral) range at room temperature extends from ∼16 to 33 mol% of Bi_2S_3. Interestingly, we could extract a 400 × 400 μm^2 rhombohedral single crystal from the sample with nominal 25 mol% Bi_2S_3. Also, in this case the EDX analysis showed a homogeneous composition, with 22 ± 1 mol% of

Bi_2S_3 and an S content exceeding the room-temperature solid solubility limit. This apparent anomaly can be explained with the phase diagram by Liu et al.[14] and the crystal growth conditions. We grew our crystals by cooling from the liquidus field. During cooling of the 25% Bi_2S_3 sample the rhombohedral phase with the eutectic composition crystallized first. Because the line separating the rhombohedral phase field from the two-phase field is temperature-dependent and shifts to higher Bi_2S_3 content with increasing the temperature, the crystallized rhombohedral phase contains more sulphur. Obviously, such state is frozen during further cooling to room temperature and results in the supersaturated Bi_2S_3–Bi_2Se_3 solid solution. This allows us to investigate the rhombohedral solid solution in the extended range up to 22 mol% Bi_2S_3.

The chemical and electronic properties of the $Bi_2Se_{3-y}S_y$ alloys were analyzed with XPS and ARPES using synchrotron

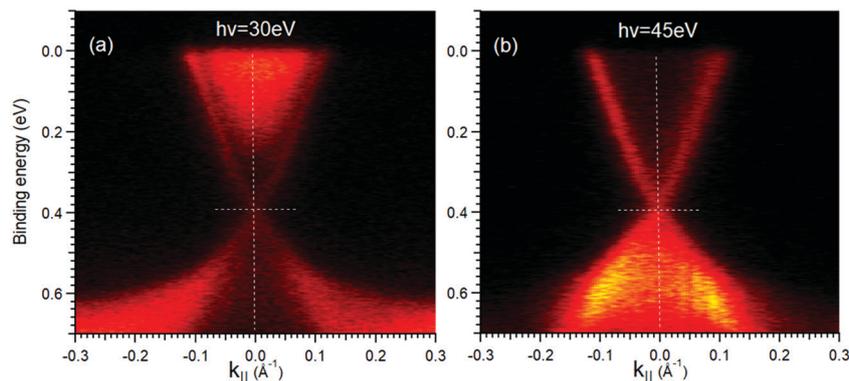This journal is © The Royal Society of Chemistry 2021

J. Mater. Chem. C, 2021, **9**, 3058–3064 | **3061**

Fig. 5 Electronic band structure of $Bi_2Se_{2.68}S_{0.32}$ near E_F measured with (a) $h\nu$ = 30 eV and (b) $h\nu$ = 45 eV. $k_{\parallel}$ = 0 Å^{-1} represents the Γ point. The chosen photon energies do not change the dispersion of the TSS, but strongly modulate the intensity of the surface and bulk features.

radiation. The spot sizes used for the XPS and ARPES analyses are of $\sim 200 \times 50$ μm^2 and $\sim 150 \times 50$ μm^2, respectively. Chemically homogeneous crystals, with areas larger than the spot sizes have been characterized *ex situ* by SEM-EDX before and after the photoemission experiments. From here on, samples are indicated by their chemical composition obtained by the EDX analysis (see Table 1) according to formula $Bi_2Se_{3-y}S_y$. During the photoemission experiments, the crystalline structure of the sample surfaces was checked by means of LEED. For S content in the $0 < y \leq 0.66$ range we observed sharp spots forming a hexagonal diffraction pattern like that of Bi_2Se_3 (Fig. 2). This is indicative that our preparation gives rise to large and crystallographically ordered domains exposing the (0001) plane of the rhombohedral phase. According to the threefold symmetry of the Bi_2Se_3 (0001) surface (plane group *p3m1*) two sets of reflections with different intensity are expected in the LEED pattern,[19] in contrast to our experimental pattern. A possible explanation for this behavior is that the electron energy of 66 eV minimizes the intensity contrast between the non-equivalent first order reflections. Alternatively, the presence of stacking faults in the crystal can produce 180° rotated domains,[20] and then result in a hexagonal pattern. The latest scenario is more frequent in epitaxially grown films than in bulk crystals. The LEED pattern of the orthorhombic phase (not shown) has rectangular symmetry.

An insight into the chemical properties of the surface of different solid solutions was obtained by XPS (Fig. 5). The binding energy (BE) of Bi 4f$_{7/2}$ (158.0 eV), Se 3d$_{5/2}$ (53.3 eV), Se 3s (228.5 eV), and S 2s (225.0 eV) does not change as a function of S content and corresponds to that of Bi, Se and S atoms in Bi_2Se_3[21] and Bi_2S_3.[22] This is an indication that S prevalently substitutes Se in Bi_2Se_3, and does not form clusters or an inhomogeneous distribution as proposed in ref. 15 to explain the anomalous transport properties of the $Bi_2Se_{3-y}S_y$ alloys.

Fig. 4 reports the electronic band structure measured near the Fermi level (E_F). All $Bi_2Se_{3-y}S_y$ compounds with $0 \leq y \leq 0.66$ possess two linearly dispersive bands crossing at Γ at 0.31 ± 0.045 eV BE. They have a surface character, as their dispersion does not change as a function of the photon energy

(see Fig. 5).[23,24] We identify these features as TSSs and their crossing as the Dirac point (DP). A DP below E_F is an indication of electron doping caused by defects.[24] The variation of the DPs within ± 45 meV can be due to slightly different concentration of intrinsic defects in the samples. These changes do not depend in a monotonic way on the S content and so are not assigned to S-driven doping effects. TSSs disappear at the composition Bi_2Se_2S, which is purely orthorhombic (magenta spectrum in Fig. 1(a)) and expected to exhibit the electronic properties of a trivial insulator.

The systematic ARPES measurements clearly show that TSSs are not destroyed by diluting Bi_2Se_3 with Bi_2S_3 as long as the rhombohedral crystal symmetry is maintained. In the $Bi_2Se_{3-y}S_y$ this is possible up to $y = 0.66$. For higher S content, it is impossible to obtain a thermodynamically stable rhombohedral structure.

Fig. 6 reports the spin analysis of the electronic structure of the $Bi_2Se_{3-y}S_y$ samples. The spin-resolved measurements are carried out with the VLEED-B polarimeter in the in-plane magnetization configuration. In this configuration, the measured Energy Distribution Curves for the two opposite directions of the target magnetization m (EDC$_{m\uparrow\downarrow}$) are used to calculate the in-plane spin polarization P using the formula $P = \dfrac{1}{S}\dfrac{EDC_{m\uparrow} - EDC_{m\downarrow}}{EDC_{m\uparrow} + EDC_{m\downarrow}}$, where $S = 0.3$ is the effective Sherman function.[18] The EDC$_{m\uparrow\downarrow}$ were collected in the two $\Delta k_{\parallel}$ intervals centered at k_p and k_n and of width 0.048 Å^{-1}, which are indicated by dashed lines in Fig. 4. We point out that k_p and k_n are non-symmetric with respect to Γ. The spin-resolved electron distribution curves (SEDCs) extracted from the measured EDC$_{m\uparrow\downarrow}$ using the formula $\dfrac{(1 \pm P)(EDC_{m\uparrow} + EDC_{m\downarrow})}{2}$ are reported in Fig. 6(a–h). The corresponding spin polarizations P are reported in Fig. 6(i–l).

In all SEDCs there are two features: one between ~ 0.3 eV BE and E_F, and another one between ~ 0.3 and ~ 0.7 eV BE. The first feature is entirely ascribed to the upper branch of the TSS and displays the expected reversal of P at the opposite sides of Γ. The behaviour of the second feature is less clear due to the overlap of the lower branch of the TSS with the bulk valence

3062 | *J. Mater. Chem. C*, 2021, **9**, 3058–3064

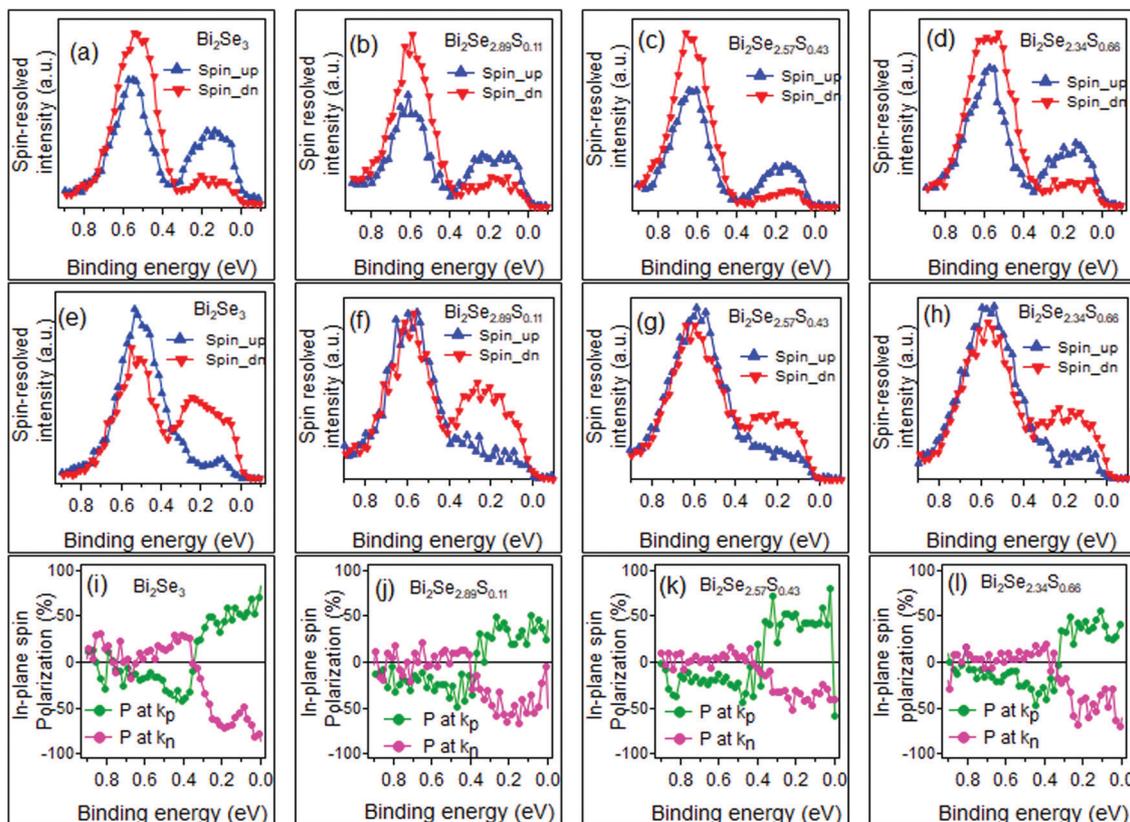This journal is © The Royal Society of Chemistry 2021

Fig. 6 (a–d) Spin-resolved electron distribution curves extracted from the $EDC_{m\uparrow\downarrow}$ measured at k_p and (e–h) at k_n on different $Bi_2Se_{3-y}S_y$ samples. The corresponding in-plane spin polarizations P at k_p (green) and P at k_n (magenta) are shown in (i–l). All the spectra were measured at photon energy 50 eV at T = 78 K.

states, which tends to reduce P, and the asymmetric acquisition geometry. For pure Bi_2Se_3, P is much lower at k_n than at k_p (Fig. 6(i)). This is even more clear for the S containing samples (Fig. 6(j–l)), where P approaches zero for k_n but is finite for k_p. However, these spurious effects do not hide the overall similar spin structure for the $Bi_2Se_{3-y}S_y$ samples with $0 \leq y \leq 0.66$.

In summary, high quality single crystals of $Bi_2Se_{3-y}S_y$ could be prepared with the Bridgman method. The ARPES and spin-resolved ARPES measurements unambiguously show that the $Bi_2Se_{3-y}S_y$ solid solution supports a spin-polarized TSS for S content in the range $0 \leq y \leq 0.66$. For these compositions, it is possible to isolate rhombohedral single crystals having homogeneous structural and chemical properties over an area of hundreds of μm.[2] The core level spectra show that upon S incorporation, Bi is 3+, Se and S are 2− and no metallic species are formed. This is an indication that S most likely substitutes Se in Bi_2Se_3 and does not form clusters or an inhomogeneous distribution as proposed by ref. 15. With S incorporation the DP of Bi_2Se_3 does not shift systematically. As soon as the structure changes from rhombohedral to orthorhombic, the material becomes a trivial insulator.

Conflicts of interest

There are no conflicts to declare.

Acknowledgements

References

1 C. L. Kane and E. J. Mele, *Phys. Rev. Lett.*, 2005, **95**, 226801.
2 A. R. Mellnik, J. S. Lee, A. Richardella, J. L. Grab, P. J. Mintun, M. H. Fischer, A. Vaezi, A. Manchon, E. A. Kim, N. Samarth and D. C. Ralph, *Nature*, 2014, **511**, 449–451.
3 W. G. Vandenberghe and M. V. Fischetti, *Nat. Commun.*, 2017, **8**, 14184.
4 J. W. McIver, D. Hsieh, H. Steinberg, P. Jarillo-Herrero and N. Gedik, *Nat. Nanotechnol.*, 2012, 7, 96–100.
5 P. Di Pietro, M. Ortolani, O. Limaj, A. Di Gaspare, V. Giliberti, F. Giorgianni, M. Brahlek, N. Bansal, N. Koirala, S. Oh, P. Calvani and S. Lupi, *Nat. Nanotechnol.*, 2013, **8**, 556–560.
6 J. Xiao, L. Kou, C. Y. Yam, T. Frauenheim and B. Yan, *ACS Catal.*, 2015, **5**, 7063–7067.

This journal is © The Royal Society of Chemistry 2021

J. Mater. Chem. C, 2021, **9**, 3058–3064 | **3063**

7 M. Neupane, S. Basak, N. Alidoust, S. Y. Xu, C. Liu, I. Belopolski, G. Bian, J. Xiong, H. Ji, S. Jia, S. K. Mo, M. Bissen, M. Severson, H. Lin, N. P. Ong, T. Durakiewicz, R. J. Cava, A. Bansil and M. Z. Hasan, *Phys. Rev. B: Condens. Matter Mater. Phys.*, 2013, **88**, 165129.

8 Z. Ren, A. A. Taskin, S. Sasaki, K. Segawa and Y. Ando, *Phys. Rev. B: Condens. Matter Mater. Phys.*, 2010, **82**, 241306.

9 L. Bao, L. He, N. Meyer, X. Kou, P. Zhang, Z. G. Chen, A. V. Fedorov, J. Zou, T. M. Riedemann, T. A. Lograsso, K. L. Wang, G. Tuttle and F. Xiu, *Sci. Rep.*, 2012, **2**, 726.

10 H. Ji, J. M. Allred, M. K. Fuccillo, M. E. Charles, M. Neupane, L. A. Wray, M. Z. Hasan and R. J. Cava, *Phys. Rev. B: Condens. Matter Mater. Phys.*, 2012, **85**, 201103.

11 H. Lin, T. Das, L. A. Wray, S. Y. Xu, M. Z. Hasan and A. Bansil, *New J. Phys.*, 2011, **13**, 095005.

12 X. Ma, D. Chang, C. Zhao, R. Li, X. Huang, Z. Zeng, X. Huang and Y. Jia, *J. Mater. Chem. C*, 2018, **6**, 13241–13249.

13 M. Beglaryan and N. K. Abrikosov, *Dokl. Akad. Nauk SSSR*, 1959, **128**, 345–347.

14 H. Liu, C. R. Knowles and L. L. Y. Chang, *Can. Mineral.*, 1995, **33**, 115–128.

15 R. Singh, V. K. Gangwar, D. D. Daga, A. Singh, A. K. Ghosh, M. Kumar, A. Lakhani, R. Singh and S. Chatterjee, *Appl. Phys. Lett.*, 2018, **112**, 102401.

16 H. Huang, J. Gu, M. Tan, Q. Wang, P. Ji and X. Hu, *Sci. Rep.*, 2017, **7**, 45565.

17 M. Neupane, S. Y. Xu, L. A. Wray, A. Petersen, R. Shankar, N. Alidoust, C. Liu, A. Fedorov, H. Ji, J. M. Allred, Y. S. Hor, T. R. Chang, H. T. Jeng, H. Lin, A. Bansil, R. J. Cava and M. Z. Hasan, *Phys. Rev. B: Condens. Matter Mater. Phys.*, 2012, **85**, 235406.

18 C. Bigi, P. K. Das, D. Benedetti, F. Salvador, D. Krizmancic, R. Sergo, A. Martin, G. Panaccione, G. Rossi, J. Fujii and I. Vobornik, *J. Synchrotron Radiat.*, 2017, **24**, 750–756.

19 X. Guo, Z. J. Xu, H. C. Liu, B. Zhao, X. Q. Dai, H. T. He, J. N. Wang, H. J. Liu, W. K. Ho and M. H. Xie, *Appl. Phys. Lett.*, 2013, **102**, 151604.

20 S. Roy, H. L. Meyerheim, K. Mohseni, A. Ernst, M. M. Otrokov, M. G. Vergniory, G. Mussler, J. Kampmeier, D. Grützmacher, C. Tusche, J. Schneider, E. V. Chulkov and J. Kirschner, *Phys. Rev. B: Condens. Matter Mater. Phys.*, 2014, **90**, 155456.

21 V. V. Atuchin, V. A. Golyashov, K. A. Kokh, I. V. Korolkov, A. S. Kozhukhov, V. N. Kruchinin, S. V. Makarenko, L. D. Pokrovsky, I. P. Prosvirin, O. K. N. Romanyuk and O. E. Tereshchenko, *Growth*, 2011, **3**, 5507–5514.

22 J. Grigas, E. Talik and V. Lazauskas, *Phys. Status Solidi*, 2002, **230**, 220–230.

23 J. Sánchez-Barriga, I. Aguilera, L. V. Yashina, D. Y. Tsukanova, F. Freyse, A. N. Chaika, C. Callaert, A. M. Abakumov, J. Hadermann, A. Varykhalov, E. D. L. Rienks, G. Bihlmayer, S. Blügel and O. Rader, *Phys. Rev. B*, 2018, **98**, 235110.

24 Z. H. Pan, E. Vescovo, A. V. Fedorov, D. Gardner, Y. S. Lee, S. Chu, G. D. Gu and T. Valla, *Phys. Rev. Lett.*, 2011, **106**, 257004.

3064 | *J. Mater. Chem. C*, 2021, **9**, 3058–3064

This journal is © The Royal Society of Chemistry 2021